Hydrogen Bonding, π-Stacking, and Aurophilic Interactions in Two Dicyanoaurate(I)-Based Manganese(II) Complexes with Auxiliary Bis-Pyridine Ligands

Chemistry Europe
European Chemical Societies Publishing

WILEY VCH

Excellence in Chemistry Research

Announcing our new flagship journal

- Gold Open Access
- Publishing charges waived
- Preprints welcome
- Edited by active scientists

Meet the Editors of *ChemistryEurope*

Luisa De Cola
Università degli Studi di Milano Statale, Italy

Ive Hermans
University of Wisconsin-Madison, USA

Ken Tanaka
Tokyo Institute of Technology, Japan

ChemPlusChem

Research Article
doi.org/10.1002/cplu.202300052

Chemistry Europe
European Chemical Societies Publishing

www.chempluschem.org

Special Collection

Hydrogen Bonding, π-Stacking, and Aurophilic Interactions in Two Dicyanoaurate(I)-Based Manganese(II) Complexes with Auxiliary Bis-Pyridine Ligands

Alessia Giordana,[a] Rosa M. Gomila,[b] Roberto Rabezzana,[a] Enzo Laurenti,[a] Emanuele Priola,*[a] Bagher Eftekhari-Sis,[c] Ghodrat Mahmoudi,*[c, d] and Antonio Frontera*[b]

The relevance of hydrogen-bonding, π-π stacking and aurophilic interactions in the solid-state of two new heterobimetallic (Au^{I}–Mn^{II}) complexes is analyzed in this manuscript. They are discrete complexes of formulae $[Mn(bipy)_2(H_2O)\{Au(CN)_2\}][Au(CN)_2]$ and $[Mn(dmbipy)_2\{Au(CN)_2\}]\cdot H_2O$, (bipy = 2,2′-bipyridine and dmbipy = 5,5′-dimethyl-2,2′-bipyridine), which are based on dicyanidoaurate(I) groups and 2,2′-bipyridyl-like co-ligands. They have been synthesized in good yields and X-ray characterized. In both compounds, aurophilic, OH···N hydrogen bonding and π-π interactions governed the supramolecular assemblies in the solid state. These contacts with special emphasis on the aurophilic interactions have been studied using density functional theory calculations and characterized using the quantum theory of atoms-in-molecules and the noncovalent interaction plot. The aurophilic contacts have been also rationalized from an orbital point of view using the natural bond orbital methodology, evidencing stabilization energies up to 5.7 kcal/mol. Moreover, the interaction energies have been decomposed using the Kitaura-Morokuma energy decomposition analysis, confirming the importance of electrostatic and orbital effects.

Introduction

The study and rationalization of supramolecular architectures is an area of great interest.[1] The inspection of X-ray structures and their packing usually reveals fascinating assemblies, which in many cases are inspiration in crystal engineering, to design solid that could find applications in different fields, as host-guest chemistry and catalysis. The hydrogen bonding interaction is the dominant force in this field,[2] though other forces like π-stacking[3] and σ-hole interactions[4] are also becoming prominent players in crystal engineering and supramolecular chemistry.

Closed-shell intermolecular interactions between gold(I) ions, namely aurophilic interactions, are also very relevant in inorganic crystal engineering and they are able to control the supramolecular dimensionality in inorganic solids.[5] In fact, the chemistry of Au(I) is replete of systems where Au···Au interactions have been described and their role in generating supramolecular assemblies highlighted.[6] It has been also demonstrated that this type of interaction can be equivalent in strength to a moderately strong hydrogen bond (~8 kcal/mol).[6,7] The linear dicyanidoaurate anion $[Au(CN)_2]^-$ is an interesting building block since it presents a dual behaviour. That is, it can act as a bridging ligand connecting transition metal atoms[8] for the construction of multidimensional frameworks and it can be involved in self-association through aurophilic interactions.[9] Several studies have shown that $[Au(CN)_2]^-$ and their complexes can aggregate in the solid state and in solution.[10] Interestingly, it has been demonstrated that the aggregation of $[Au(CN)_2]^-$ anion causes variations in the luminescence and such phenomenon has been used for monitoring biological processes.[11] Moreover, the $[Au(CN)_2]^-$ anion combined with other transition metal ions and auxiliary ligands have been used in inorganic-organic crystal engineering, constructing new supramolecular assemblies with interesting luminescence properties. The analysis of optical properties is not the purpose of the present work that is more focused on

[a] Dr. A. Giordana, R. Rabezzana, E. Laurenti, Dr. E. Priola
Department of Chemistry
Università degli Studi di Torino
Via Pietro Giuria 7
10125 Torino (Italy)
E-mail: Emanuele.priola@unito.it
[b] Dr. R. M. Gomila, A. Frontera
Department of Chemistry
Universitat de les Illes Balears
Crta de Valldemossa km 7.5
07122 Palma de Mallorca (Spain)
E-mail: toni.frontera@uib.es
[c] Prof. B. Eftekhari-Sis, Prof. G. Mahmoudi
Department of Chemistry
Faculty of Science
University of Maragheh
P.O. Box 55136–83111
Maragheh (Iran)
E-mail: ghodratmahmoudi@gmail.com
[d] Prof. G. Mahmoudi
Samara State Technical University,
Molodogvardeyskaya Str 244
Samara 443100 (Russia)

Supporting information for this article is available on the WWW under https://doi.org/10.1002/cplu.202300052

Part of a Special Collection on "Gold Chemistry"

the analysis of the noncovalent interactions, as detailed in the following sections.[12,13]

Here, we report the synthesis, spectroscopic and X-ray characterization of two new heterobimetalic (Au^{I}–Mn^{II}) complexes using 2,2′-bipyridine (bipy) and 5,5′-dimethyl-2,2′-bipyridine (dmbipy) as auxiliary co-ligands, namely, $[Mn(bipy)_2(H_2O)\{Au(CN)_2\}][Au(CN)_2]$ (**1**) and $[Mn(dmbipy)_2\{Au(CN)_2\}]\cdot H_2O$ (**2**). The assemblies, constructed by cooperative hydrogen bonding, π-π stacking and aurophilic interactions, have been described and studied using DFT calculations, molecular electrostatic potential (MEP) surface analysis and two methods based on the topology of the electron density, QTAIM[14] and NCIplot.[15] Moreover, the donor-acceptor orbitals involved in the aurophilic interaction are analyzed using the natural bond orbital (NBO) methodology[16] and the Kitaura-Morokuma[17] energy decomposition analysis. These methods have been used (and criticized) before to analyse aurophilic interactions.[5–8,18]

Results and Discussion

As shown in Scheme 1, compounds **1** and **2** are discrete heterometallic complexes. As commented above, the $[Au(CN)_2]^-$ anion usually acts as bridging ligand where both ends of the linear anion are coordinated to metal centers promoting in many cases the generation of coordination polymers instead of discrete complexes. We have initially searched the CSD and found only 18 structures in the data base including Mn^{II}–Au^{I} heterometalic complexes involving the $[Au(CN)_2]^-$ anion. Agreeably, 12 out of 18 are polymeric and the monomeric unit propagates due to the bidentate nature of the dicyanoaurate. Only 6 structures are discrete complexes like those reported herein, thus emphasizing the lack of the type of complexes reported in this manuscript.

Description of the structures

The X-ray diffraction study of complex **1** shows that the compound crystallizes in monoclinic space group $P2_1/c$. Figure 1 depicts the asymmetric unit consisting of a $[Mn(bipy)_2(H_2O)\{Au(CN)_2\}]$ complex cation and a cyanoaurate species that guarantees the electroneutrality of the compound. A selection of bond lengths and angles is reported in Table 1. The manganese(II) atom exhibits a distorted octahedral coordination sphere built by the chelating bipy ligands, a cyano group from a cyanoaurate anion, and an aquo ligand. The Mn–N(bipy) bond lengths vary from 2.237(4) to 2.287(4)Å, while the Mn–N4(cyano) bond is slightly shorter (2.199(5)Å), and the $Mn–OH_2$ is even shorter, of 2.140(3) Å. The bipy mean planes form a dihedral angle of 81.9°. The Au–C bond lengths are similar, comparable within their estimated standard deviations.

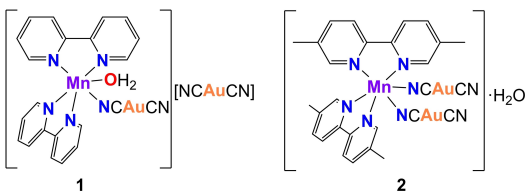

Scheme 1. Compounds **1** (left) and **2** (right) synthesized in this work.

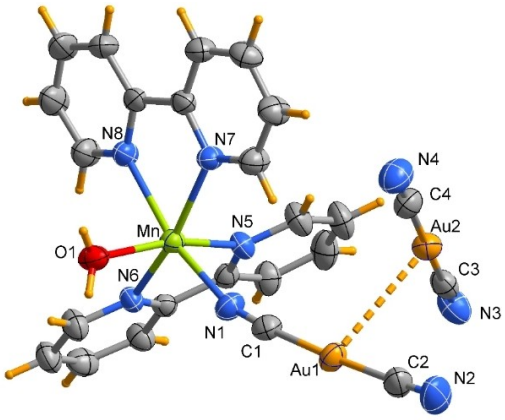

Figure 1. ORTEP drawing (ellipsoids at 40% probability) of the asymmetric unit of complex **1**.

Table 1. Selected coordination bond lengths (Å) and angles (°) for compounds **1** and **2**.

Labels	1	2
Au1–C1	1.970(6)	1.93(2)
Au1–C2	1.970(6)	1.97(3)
Au2–C3	1.985(6)	1.93(2)
Au2–C4	1.970(7)	1.98(2)
Mn–O1	2.142(3)	–
Mn–N3	–	2.208(15)
Mn–N1	2.198(5)	2.196(19)
Mn–N5	2.237(4)	2.239(13)
Mn–N6	2.247(3)	2.201(14)
Mn–N7	2.272(4)	2.245(14)
Mn–N8	2.287(4)	2.276(15)
N5–Mn–N6	72.61(13)	73.4(5)
N7–Mn–N8	72.20(14)	71.5(6)
N5–Mn–O1	163.54(13)	–
N5–Mn–N3	–	166.8(5)
N6–Mn–N7	161.44(15)	166.8(5)
N1–Mn–N8	164.03(14)	161.3(6)

The crystal packing analysis evidenced the formation of zig-zag polymeric chains realized by unsupported aurophilic Au1···Au2 interactions (with alternating distances of 3.2603(3) and 3.7009(3)Å, Figure 2). Moreover, the coordinated water molecules expand the dimensionality to a layered 2D network by means of H-bonds with the cyano nitrogen atoms N2 and N4 of symmetry related complexes, with O···N distance of 2.76Å. All H-bond parameters are reported in Table S1. Moreover, π···π interactions are present among the py rings of nearby cation complexes forming self-assembled dimeric structure (Table S2).

Complex **2** crystallizes in monoclinic space group *I*2/*a* and the asymmetric unit comprises a discrete $[Mn(dmbipy)_2\{Au(CN)_2\}_2]$ complex and a water molecule located on a center of symmetry. An Ortep drawing of the crystallographic asymmetric unit is reported in Figure 3, and a selection of bond lengths and angles are collected in Table 1. Here both cyanoaurate anions are coordinated to the manganese atom, while the water

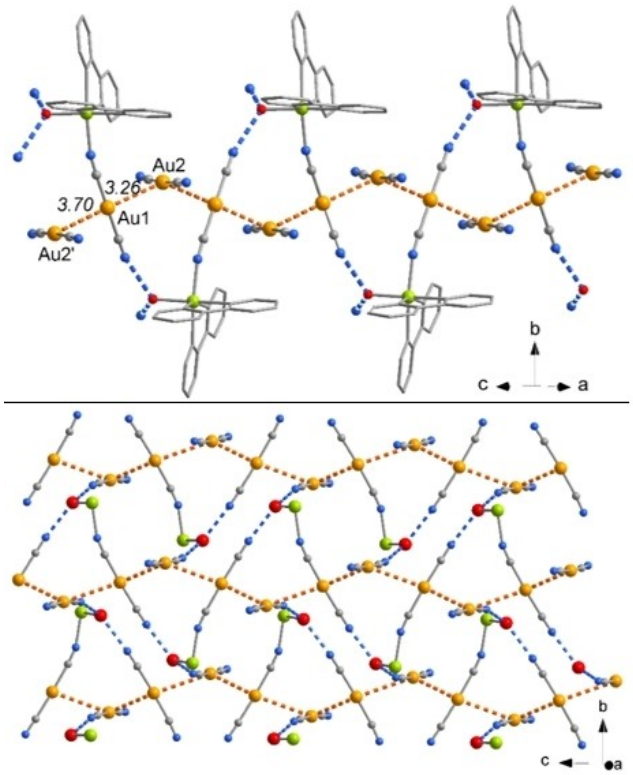

Figure 2. Top: polymeric structure of complex **1** built by aurophilic interactions (dotted orange lines) and H-bonds (blue dotted lines). Distances in Å. Bottom: the 2D polymeric structure of complex **1** built by the lattice water molecules through OH···N hydrogen bonds (blue dotted lines) and Au···Au interactions (orange dotted lines). The bipy ligands not shown for sake of clarity.

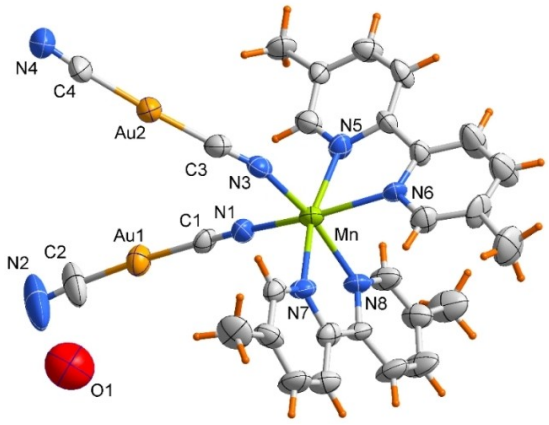

Figure 3. ORTEP drawing (ellipsoids at 30% probability) of the asymmetric unit of complex **2.**

molecule is present as a lattice species. Replacement of the bipy ligand with the correspondent dimethyl derivative leads to a complex isomeric to **1**. The coordination bond lengths and angles, although at lower accuracy, agree with those found in complex **1**.

It is worth noting the peculiar packing: complexes interdigitate in pair referred by a 2-fold crystal axis (as displayed in Figure 4). This adduct is held together by unsupported aurophilic interactions, with comparable Au1···Au1′ and Au1···Au2′ distances of 3.3709(17) and 3.3988(10)Å respectively, and the four $[Au(CN)_2]^-$ anions exhibit a staggered arrangement (see Scheme 2) with angles at Au1 of 123.75(3)°. The crystal packing evidences the formation of polymeric chains (Figure 5) developing along axis *a* where the dimeric adducts are connected by the lattice water molecules through H-bonds with cyano N2 of symmetry related complexes (O1···N2 of 2.88(3)Å). A 2D polymeric structure is constructed by π···π interactions between py rings, as shown in Figure 5.

Spectroscopic characterization

The vibrational features of compounds **1** and **2** have been investigated by IR spectroscopy and relative spectra are depicted in Figure S1. Spectra present signals related to aromatic ligand modes in the fingerprint range (1650–700 cm^{-1}), to cyanide modes around 2100 cm^{-1} and to OH stretching in spectral range 3600–3200 cm^{-1}. The formation of the complexes can be confirmed by comparison of spectrum of ligands with the spectra of the complexes. Generally, it can be observed a shift at higher wavenumbers in the fingerprint range, and in particular the shift of the breathing modes of pyridine rings[19] is due to the major rigidity induced by metal coordination.[20] At high wavenumbers it is present for both complexes a broad band attributable to water molecule interacting through H bonding. It can be observed a more

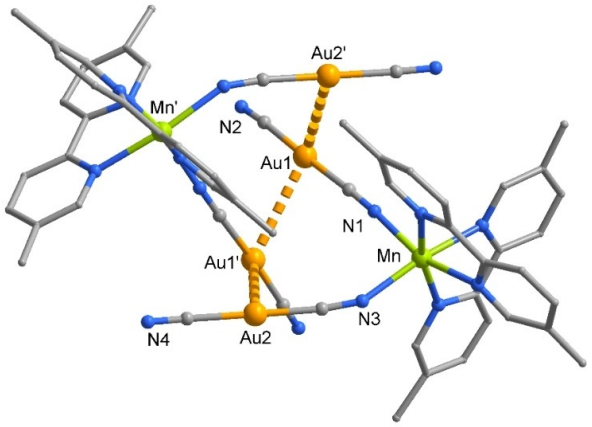

Figure 4. Molecular structure of the dimeric $[Mn(dmbipy)_2\{Au(CN)_2\}_2]_2$ adduct of complex **2**. Primed atoms at −x+1/2, y, −z+1. Lattice water molecule and H atoms not shown for clarity.

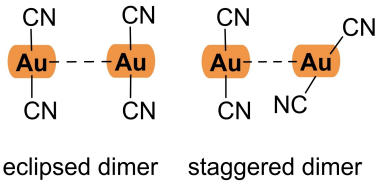

Scheme 2. Possible geometrical arrangement of aurophilic interactions in $Au(CN)_2^-$ anion dimers.

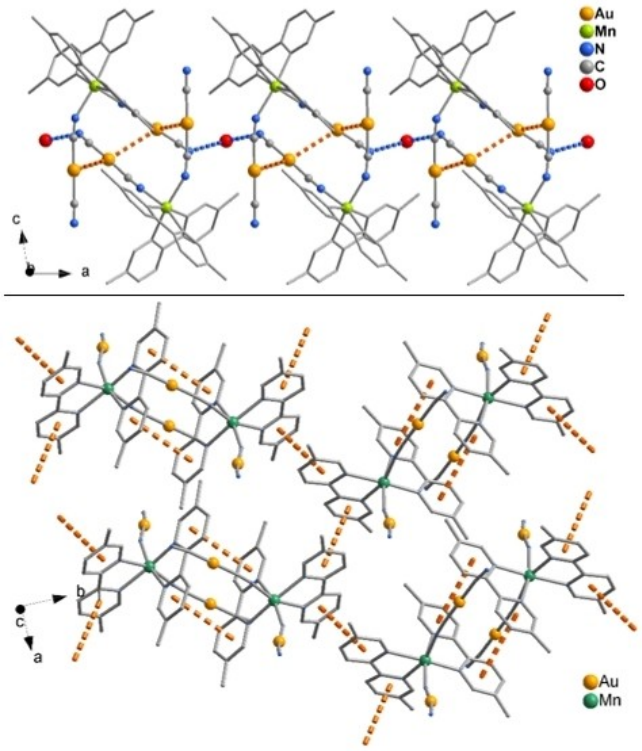

Figure 5. Top: Supramolecular polymeric structure of complex **2** built by a lattice water molecule (big red sphere) connecting the dimeric $[Mn(dmbipy)_2\{Au(CN)_2\}_2]_2$ adduct through OH···N hydrogen bonds. Bottom: 2D polymeric structure of complex **2** constructed by π···π interactions.

structured band for complex **1**, probably related to coordination of water to Mn(II) atom. Cyanide groups originate intense and well-defined signals. For complex **1** the strong peak at 2141 cm^{-1} is attributable to the non-coordinated Au(CN) units, while the signal of bridging cyanide shift at higher wavenumber (2160 cm^{-1}) due to coordination.[21] Bridging cyanide groups are very sensible to the environments and it has been reported a correlation between the number of ν(CN) bands and the number of inequivalent cyanide groups in the structure.[22] In fact in complex **2** two signals are present and attributable to linear and bend bridging cyanide groups (at 2174 and 2168 cm^{-1}).

The intense signals of cyanide modes are recognizable in ATR spectra of very concentrated methanolic solution of complexes. It is possible to observe a sligh shift and broadening of signals for complexes **1** and **2** (in Figure S2), suggesting that the structural unit observed in the solid state, is present also in solution. EPR data indicate that in ethanolic solution Mn(II) atom has an octahedral coordination sphere. (in Figure S3) These experimental results suggest that non-covalent interactions observed in the solid state, especially aurophilic interactions, are present also in solution, as supported by a previous study on Zn–Au nucleation units.[23] To confirm this hypothesis, ethanolic solutions of both complexes were investigated by electrospray ionization mass spectrometry (ESI-MS). Full scan spectra are reported for complexes **1** and **2** in Figure S4 and S5, respectively.

In Figure S4, the most abundant peaks are assigned to interactions of the free bipy ligand with cations typically present in the ESI environment, namely: $[bipy+H]^+$ ($m/z=157$), $[bipy+Na]^+$ ($m/z=179$), ans $[bipy+K]^+$ ($m/z=195$). The molecular ion of complex **1** is absent; however, a peak at $m/z=479$ is clearly detectable, and is assigned to the $[Mn(H_2O)(bipy)(Au(CN)_2)H]^+$ ion. This ion is likely yielded by loss of a single bipy molecule from the molecular ion and shows that water is indeed directly coordinated to the Mn metal center.

The full scan spectrum of complex **2** indicates that the molecular ion loses a dicyanoaurate ligand to form the $[Mn(dmbipy)_2(Au(CN)_2)]^+$ ion ($m/z=672$). Consecutive losses of both dmbipy ligands give rise to the $[Mn(dmbipy)(Au(CN)_2)]^+$ ion ($m/z=488$) and to $[Mn(Au(CN)_2)]^+$ ($m/z=304$). The peak at $m/z=488$ is barely detectable in the full scan spectrum, but MS/MS experiments (not reported) performed on the $[Mn(dmbipy)_2(Au(CN)_2)]^+$ ion display an abundant peak at $m/z=488$, which confirms this ligand loss. Also for complex **2**, the most abundant peaks are attributable to interactions of the free ligand with H^+ ($[dmbipy+H]^+$, $m/z=185$), Na^+ ($[dmbipy+Na]^+$, $m/z=207$; $[(dmbipy)_2Na]^+$, $m/z=391$), and K^+ ($[dmbipy+K]^+$, $m/z=223$). However, the other signals highlighted for both full scan mass spectra clearly indicate that both complexes are stable in solution phase.

Theoretical analysis

First, we have computed the MEP surfaces of both compounds to investigate the most electron rich and electron poor parts of the molecules. In case of compound **1**, we have used the ion-pair where the dicyanidoaurate anion is H-bonded to the Mn(II)-coordinated water molecule in order to use a neutral system. The MEP surfaces are represented in Figure 6, disclosing that the MEP minimum in **1** is located at the N-atom of the H-bonded dicyanidoaurate anion (−71 kcal/mol) followed by the N-atom of the coordinated one (−62 kcal/mol). In compound **2**, the minima are located at the N-atoms of the coordinated dicyanoaurate anions (−70 kcal/mol). In **1**, the MEP maximum is located at the H-atom of the coordinated water molecule (+

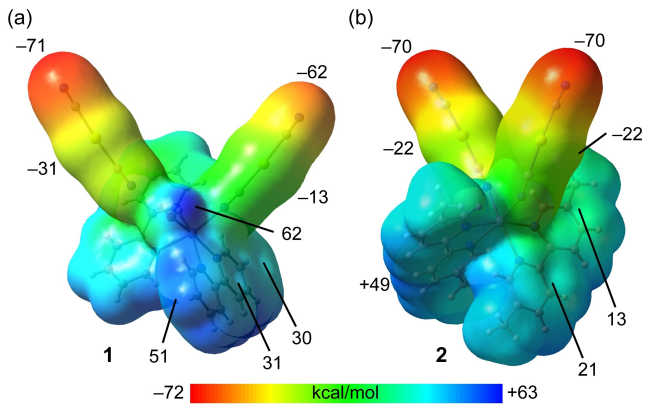

Figure 6. MEP surfaces (isovalue 0.001 a.u.) of compounds **1** (a) and **2** (b). Values at selected points are indicated in kcal/mol.

62 kcal/mol) and in **2** at the aromatic H-atoms of the dmbpy ligand (+49 kcal/mol). The MEP values are also positive over the centers of the aromatic rings ranging from +13 to +31 kcal/mol (respectively in **2** and **1**). The MEP also reveals the nucleophilic nature of the Au(I) atoms with MEP values ranging from −13 to −31 kcal/mol.

The selection of the fragments used in the DFT study is based on the assemblies described in Figures 1, 2, 4 and 5, that are crucial governing the crystal packing and solid state architecture of compounds **1** and **2**.

Figure 7a shows the combined QTAIM/NCIplot analysis of the H-bonded assembly of compound **1**. Both methods combined are useful to reveal interactions in real space and to know their attractive or repulsive nature. The colour used in these representations for the reduced density gradient (RDG) isosurfaces depends on the sign of the middle eigenvalue of ϱ (λ_2) and the magnitude of ϱ. In the NCIPlot representations shown in this manuscript we have used blue for strong and attractive interactions and green for weak and attractive interactions. As shown above in Figure 2 (bottom), the Mn(II)-coordinated water molecule establishes two H-bonds (HBs), one with the counterion and another one with the coordinated dicyanidoaurate ligand, thus generating the 2D polymeric structure in cooperation with the aurophilic Au(I)···Au(I) interactions. Both contacts are revealed by the QTAIM/NCIplot analysis, showing a bond critical point (CP, represented as a small red sphere) and bond path (represented as orange line) connecting one N-atom of the dicyanidoaurate anion to the H-atom of water (in Figure 7). Each HB is further characterized by a dark blue RDG isosurface, that coincides to the location of the bond CP, thus revealing the strong nature of these H-bonding interactions. The QTAIM/NCIplot analysis also discloses the existence of an anion-π interaction between the noncoordinated dicyanidoaurate anion and the π-system of the bipy ligand, in line with the MEP analysis that showed large and positive MEP values over the aromatic rings. The anion-π interaction is characterized by a bond CP and a bond path connecting the N-atom to one C-atom of the ring, and by a more extended green isosurface that embraces most of the π-cloud of one pyridine ring, as typical in π-interactions.

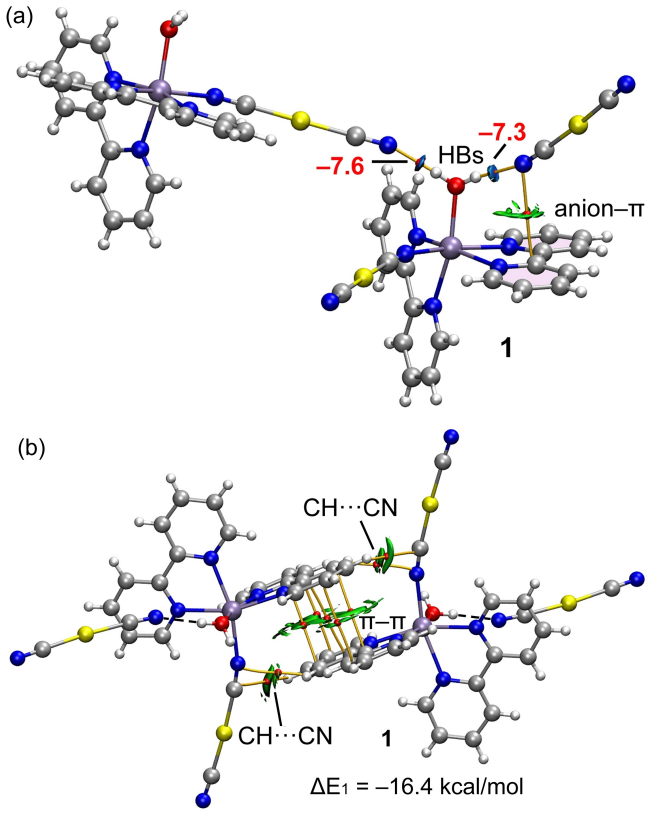

Figure 7. QTAIM/NCIplot analysis of the H-bonded assembly (a) and centrosymmetric π-stacked dimer (b) of **1**. Only intermolecular interactions are represented. See theoretical methods for the NCIPlot settings. The energies of the H-bonds (HBs) are indicated in red, close to the bond CPs.

The strength of each HB has been estimated using the value of the potential energy density at the bond CPs and the formula proposed by Espinosa et al.[24] This is very convenient method to estimate the strength of the HBs free from the strong electrostatic effects due to the ion-pair nature of the interaction. The energies of the HBs, indicated in red in Figure 7a, are large and very similar (−7.3 kcal/mol for the noncoordinated dicyanidoaurate anion and −7.6 kcal/mol for the coordinated one) demonstrating the importance of these contacts in the solid state organization of compound **1**. Figure 7b shows the QTAIM/NCIplot analysis of the π-stacked self-assembled dimer extracted from the X-ray packing. The π···π interaction is characterized by five bond CPs and bond paths interconnecting the bipy ligands. Moreover, the interaction is further characterized by an extended RDG green isosurface that embraces the whole ligand, disclosing a strong complementarity. The QTAIM/NCIplot analysis also reveals the existence of additional CH···CN contacts between the aromatic H-atoms and the coordinated dicyanidoaurate ligands. The observation of such contacts agrees with the MEP surface analysis, since the MEP values at the aromatic H-atoms are large and positive (51 kcal/mol), as observed for donor site involved in HBs. As a consequence of such combination of interactions, the dimerization energy is very large ($\Delta E_1 = -16.4$ kcal/mol).

The aurophilic interactions observed in compound **1** were also analyzed using the QTAIM and NCIplot tools and also from an orbital point of view. In particular, the NBO analysis was used since it is convenient to analyze orbital donor-acceptor interactions and to disclose their stabilization energies from the second order perturbation analysis. We performed the combined QTAIM/NCIPlot analysis of a molecular fragment constituted by the cationic complex $[Mn(bipy)_2(H_2O)\{Au(CN)_2\}]^+$ interacting with two dicyanoaurate counterions, as shown in Figure 8a.

The aurophilic interactions are characterized by a bond CP and bond path interconnecting the Au atoms, thus confirming the existence of the Au(I)···Au(I) interactions. Moreover, disk-shaped green-bluish RDG isosurfaces are also located between the Au-atoms, also supporting the existence and attractive nature of the aurophilic interactions. One of the cyanoaurate units is further connected to the cationic part via CH···N, CH···Au and N···π contacts as disclosed by the distribution of bond CPs and bond paths. The binding energy of the cation complex

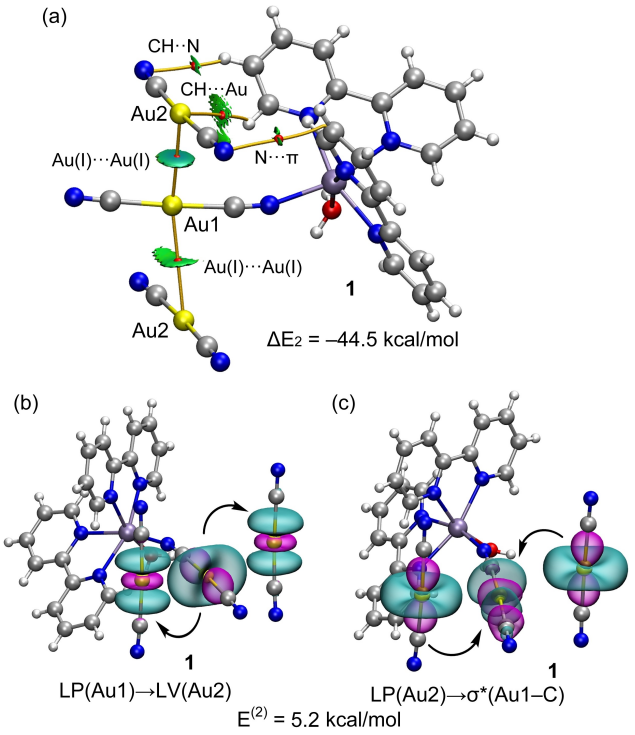

Figure 8. (a) QTAIM/NCIplot analysis of the aurophilic assembly of **1**. Only intermolecular interactions are represented. See theoretical methods for the NCIPlot settings. (b,c) Plots of the NBOs involved in the electron charge transfer and the associated stabilization energy. In the NBO terminology, LV orbital is an "unfilled valence" orbital located in an atom.

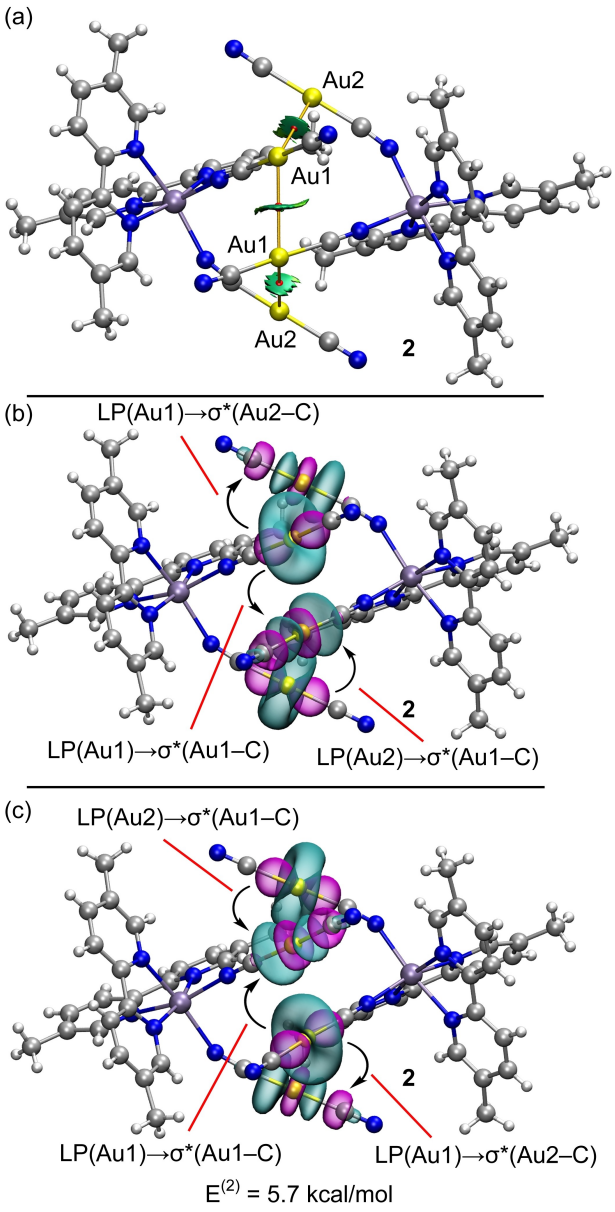

Figure 9. (a) QTAIM/NCIplot analysis of the aurophilic self-assembled dimer of **2**. Only aurophilic interactions are represented. See theoretical methods for the NCIPlot settings. (b,c) Plots of the NBOs involved in the electron charge transfer and the concomitant stabilization energy.

interacting with two $[Au(CN)_2]^-$ is very large ($\Delta E_2 = -44.5$ kcal/mol) due to the ion-pair nature of the assembly.

The NBO calculation indicate two types of orbital donor-acceptor interactions. On one hand, the NBO analysis revealed an electron donation from a lone pair (LP) orbital of Au1 (belonging to the coordinated dicyanidoaurate ligand, located at the d_z^2 orbital) to "lone vacancy" (LV) type orbitals of Au2 (belonging to the non-coordinated dicyanidoaurate anions), as represented in Figure 8b [LP(Au1)→LV(Au2)]. This empty valence nonbonding orbital (LV) has 20% of *s*-character and 80% of *d*-character. On the other hand, there is also an electron donation from the LP orbitals of Au2 atoms (located at the d_z^2 orbitals) to the antibonding σ*(Au1–C) orbital, as represented in Figure 8c [LP(Au2)→σ*(Au1–C)]. The concomitant stabilization energy due to these orbital donor-acceptor interactions is 5.2 kcal/mol, supporting the importance of aurophilic interactions in the solid state of compound **1**.

For compound **2**, we have also examined the aurophilic interactions using the combined QTAIM/NCIplot methods and the NBO analysis. Figure 9a shows the distribution of CPs and bond paths corresponding to the Au···Au interactions in the self-assembled dimer described in the previous section (see Figure 4). The presence of bond CPs, bond paths and green isosurfaces interconnecting the Au atoms confirm the existence and attractive nature of the Au(I)···Au(I) contacts. The NBO analysis evidences two types of dominant donor-acceptor interactions. That is, an LP orbital belonging to the Au1 atom donates charge to the σ*(Au1–C) orbital of the other monomer, and *vice versa* (see Figure 9b and c). The same type of donor-acceptor interaction [LP(Au)→σ*(Au–C)] is also observed for the two Au1···Au2 pairs, as represented in Figure 9b and c. The total stabilization energy due to aurophilic interactions is 5.7 kcal/mol, slightly greater than that of compound **1**.

The QTAIM parameters measured at the bond CPs that characterize the Au···Au interactions in compounds **1** and **2** are gathered in Table 2. The values are typical of weak noncovalent interactions with $\varrho < 0.02$ a.u. and $Gr \approx -Vr$. In case of compound **2**, the QTAIM parameters are similar for both contacts, indicating similar strength. In contrast, the QTAIM parameters in compound **1** for the Au1···Au2 and A1···Au2′

Table 2. Values of the charge density (ϱ), the Lagrangian kinetic energy (G_r), the potential energy density (V_r), the total energy density (H_r) and the Laplacian of the electron density ($\nabla^2\varrho$) measured at the bond CPs that characterize the Au(I)···Au(I) contacts in compounds **1** and **2**. All values in a.u. See Figures 2 and 4 for atom labels.

Labels	ϱ	G_r	V_r	H_r	$\nabla^2\varrho$
Compound **1**					
Au1–Au2	0.0190	0.0125	−0.0130	−0.0005	0.0478
Au1–Au2′	0.0086	0.0051	−0.0046	0.0006	0.0227
Compound **2**					
Au1···Au1	0.0154	0.0101	−0.0100	0.0001	0.0406
Au1···Au2	0.0146	0.0094	−0.0093	0.0001	0.0381

interactions are quite different, in line with the colours of the NCIplot isosurfaces shown in Figure 8a and confirming that the Au1···Au2 is stronger. The Laplacian values are positive in all cases, as common in closed shell interactions.[14]

Finally, to complement the NBO and QTAIM analyses, an energy decomposition analysis (EDA) study was performed for the π-stacking (Figure 7b) and aurophilic assemblies (Figure 8a and 9a) described above. The results are summarized in Table 3, showing that for the π-stacking the dominant contribution is the dispersion ($E_{disp} = -14.5$ kcal/mol) followed by the correlation ($E_{corr} = -7.3$ kcal/mol), as expected in interactions where aromatic rings are involved. Both the orbital (E_{orb}) and electrostatic (E_{ele}) terms have similar values (−5.4 and −5.3 kcal/mol, respectively)

In contrast the aurophilic assemblies present much higher electrostatic terms (see Table 3) due to the ion-pair nature of these assemblies. Moreover, the orbital and dispersion contributions are similar in the aurophilic assemblies, though in the assembly of compound **2** the values are considerable larger but compensated by a much larger exchange-repulsion term ($E_{exch-rep}$).

Conclusions

Two new Mn(II)-Au(I) discrete heterometalic complexes based on linear dicyanidoaurate anion $[Au(CN)_2]^-$ ligands/counterions and 2,2′-bipyridyl like heterocycles (bipy, dmbipy) were synthesized and structurally characterized. Due to the ionic nature of the structures, the Coulombic attraction is the predominant driving force of the formed X-ray structures, though the final assemblies are influenced by other more directional forces, as shown in this work. The supramolecular assemblies have been analyzed focusing on the interesting combination of non-covalent interactions such as hydrogen bonding, π-π, and Au···Au interactions, since they play a fundamental role governing the final crystal packing. Both the H-bonds and π-stacking interactions are energetically relevant in compound **1**. Moreover, the aurophilic interactions have been analyzed in detail, disclosing their attractive nature by using the NCIplot method. The NBO analysis discloses relevant donor-acceptor interactions, where the dominant one is an electron donation from a LP located at a d-orbital of Au(I) of one dicyanidoaurate to the empty σ*(Au–C) antibonding orbital of the adjacent dicyanidoaurate anion and *vice versa*. The total stabilization energy is similar in both complexes. It is expected that the results reported herein will be of interest for the inorganic crystal engineering and supramolecular chemistry communities as well as to advance in the understanding of the aurophilic interactions.

Table 3. Values of the electrostatic (E_{ele}), exchange repulsion(E_{ex-rep}), orbital (E_{orb}), correlation (E_{corr}) and dispersion (E_{disp}) components to the binding energies of the π-π and aurophilic assemblies of compounds **1** and **2**. All values in kcal/mol.

Labels	E_{ele}	E_{ex-rep}	E_{orb}	E_{corr}	E_{disp}
Compound **1**					
π-π	−5.4	14.2	−5.3	−7.3	−14.5
Au···Au	−23.2	7.7	−9.2	−3.2	−10.0
Compound **2**					
Au···Au	−33.9	49.3	−25.3	−15.3	−25.4

Experimental Section

Synthesis of Complexes 1 and 2

$[Mn(bipy)_2(H_2O)\{Au(CN)_2\}][Au(CN)_2]$ (**1**): A mixture of 25.5 mg (0.104mmol) of manganese(II) acetate tetrahydrate, 17.0 mg (0.108mmol) of bipy and 30.0 mg (0.104 mmol) of potassium dicyanoaurate have been added to 10 mL of boiling ethanol, and the obtained solution left under stirring for 10 min. Large transparent crystals were obtained from slow evaporation after 2 weeks, and washed with cold water. Yield: 9.3%. Elemental analysis (in %): calcd. for **1**: 32.63 C, 2.05 H, 12.63 N, 1.82 O. Exp: 32.51 C, 2.12 H, 12.72 N, 1.91 O. ATR-FTIR (cm^{-1}): 2160 m (νCN), 2141 s (νCN), 1595 m, 1575 m, 1563 m, 1475 w, 1440 m, 1410 m, 1245 w, 1155 w, 1014 w, 762 m, 735 w.

$[Mn(dmbipy)_2\{Au(CN)_2\}_2]\cdot H_2O$ (**2**): A mixture of 25.5 mg (0.104mmol) of manganese(II) acetate tetrahydrate, 19.0 mg of dmbipy (0.103 mmol) and 30.0 mg (0.104 mmol) of potassium dicyanoaurate have been added to 10 mL of boiling ethanol, and the obtained solution left under stirring for 10 min. Large transparent crystals were obtained from slow evaporation after 2 weeks and washed with cold water. Yield: 9.71%. Elemental analysis (in %): calcd. for **2**: 36.14 C, 2.71 H, 12.04 N, 0.86 O. Exp: 36.33 C, 2.67 H, 11.15 N, 1.6O. ATR-FTIR (cm^{-1}): [1]2174 m (νCN), 2168 m (νCN), 2141 vs (νCN), 1650 vw (br), 1600 w, 1573 m, 1480 m, 1385 m, 1246 w, 1233 w, 1161 w, 1043 m, 835 w, 732 w.

Single-crystal X-ray diffraction. Diffraction data of compounds **1** and **2** were collected at room temperature using an Xcalibur, Ruby, Gemini ultra-diffractometer with Mo–Kα radiation (λ = 0.71073 Å). Cell refinement, indexing, and scaling of the data sets were performed using the CrysAlisPro package of programs.[25] An empirical absorption correction was applied to the data sets.[25] The structures were solved by direct methods with SHELXS.[26] Non-hydrogen atoms were refined by full-matrix least-squares on F^2 with anisotropic displacement parameters using the SHELXL 2018/3.[26] Data of compound **2** were treated with Squeeze[27] to take into account the void of 1255.2 $Å^3$, 18.1% of the unit cell volume, likely filled by disordered solvent molecules. The contribution of H-atoms at calculated positions was included in the final cycles of refine-

ments. Crystal data and details of refinements are reported in Table S3.

Deposition Numbers 2237545 (**1**) and 2237546 (**2**) contain the supplementary crystallographic data for this paper. These data are provided free of charge by the joint Cambridge Crystallographic Data Centre and Fachinformationszentrum Karlsruhe Access Structures service.

Characterizations. Correspondence between the bulk and SC-XRD structures as well as sample purity were checked by comparison of experimental and calculated powder XRD (PXRD) pattern (see Figure S). Powder diffraction data have been collected using Xcalibur, Ruby, Gemini ultra-diffractometer with Cu–Kα radiation (λ = 1.54184 Å). The elemental analyses (C, H, N and S) were carried out using a Thermo FlashEA 1112 CHNS-O analyzer. ATR spectra were obtained with a Bruker Vertex 70 spectrometer, equipped with the Harrick MVP2 ATR cell. ESI-MS measurements were performed employing an AB Sciex 3200 Q trap mass spectrometer in positive mode in the mass range 50–1000 Da. EPR spectra were recorded with a X-band Bruker-EMX spectrometer equipped with a cylindrical cavity operating at 100 kHz field modulation (frequency 9.86 GHz; power 10 mW; modulation amplitude 4 Gauss). The ESI-MS conditions were as follows: ion spray voltage 3500 V; curtain gas pressure 20 psi; temperature 200 °C; nebulizer gas pressure 20 psi; auxiliary gas pressure 10 psi; declustering potential 20 V; entrance potential 10 V. Ethanolic solutions of complexes **1** and **2** were prepared at concentrations of 1.0×10^{-5} M, and were directly injected in the ESI ion source at 3.000 μL/min flow. Data analysis was performed by Analyst software (AB Sciex).

DFT calculations: The energy and EDA calculations were carried out using the Turbomole 7.7 program[28] and the PBE0[29]-D3[30]/def2-TZVP[31] level of theory. For gold, the def2-TZVP basis set used in this work includes effective core potentials (ECP),[32] and relativistic effects are used for the inner electrons.[31] For Mn(II) high spin configuration has been used (5 unpaired electrons for each Mn). The crystallographic coordinates have been used to evaluate the interactions in the solid state of compounds **1** and **2**, since we are interested to study the interactions as they stand in the solid state. The dimers and trimers extracted from the solid-state structures were selected to study the aurophilic interactions. The interaction energies were computed by subtracting the sum of the energies of the monomers to that of the assembly. The Bader's "Atoms in molecules" theory (QTAIM)[14] and noncovalent interaction plot (NCIPlot)[15] were used to study the interactions discussed herein using the Multiwfn program[33] and represented using the VMD visualization software.[34] The molecular electrostatic potential (MEP) surfaces were computed using the 0.001 a.u. isosurface as best estimation of the van der Waals surface at the same level of theory and represented using the GaussView program.[35] For the NCIplot representations, the following settings were used: RDG isosurface = 0.5, density cut-off = 0.04 a. u., color scale $-0.035 \leq (\mathrm{sign}\lambda_2)\varrho \leq 0.035$ a.u. Natural bond orbital (NBO)[16] calculations were performed using the NBO7.0 program.[36]

Acknowledgements

This research was funded by the "Ministerio de Ciencia, Investigacion y Universidades/Agencia Estatal de Investigación" (MICIU/AEI/10.13039/501100011033) of Spain (project PID2020-115637GB-I00. FEDER funds). We thank Prof. E. Diana for his support in IR measurements and fruitful discussion on vibrational data.

Conflict of Interests

The authors declare no conflict of interest.

Data Availability Statement

The data that support the findings of this study are available from the corresponding author upon reasonable request.

Keywords: crystal engineering · cyanides · heterometallic complexes · noncovalent interactions · supramolecular chemistry

[1] a) G. R. Desiraju, *J. Am. Chem. Soc.* **2013**, *135*, 9952–9967; b) G. R. Desiraju, *Angew. Chem. Int. Ed.* **2007**, *46*, 8342–8356.
[2] a) G. C. Pimentel, A. L. McClellan, *The Hydrogen Bond*; W. H. Freeman & Co.: San Francisco, CA, USA, **1960**; b) G. R. Desiraju, T. Steiner, *The Weak Hydrogen Bond. In Structural Chemistry and Biology*; International Union of Crystallography, Oxford Science Publications: Oxford, UK, **1999**; c) G. Gilli, P. Gilli, *The Nature of the Hydrogen Bond: Outline of a Comprehensive Hydrogen Bond Theory*; International Union of Crystallography, Oxford Science Publications: Oxford, UK, **2009**; d) S. J. Grabowski, J. Lesczcynski, (Eds.) *Hydrogen Bonding – New Insights*; Springer: Dordrecht, The Netherlands, 2006; e) Z. T. Li, L. Z. Wu (Eds.) *Hydrogen Bonded Supramolecular Structures*; Springer: Berlin/Heidelberg, Germany, 2015; f) I. Alkorta, I. Rozas, J. Elguero, *Chem. Soc. Rev.* **1998**, *27*, 163–170; g) M. Juanes, R. T. Saragi, W. Caminati, A. Lesarri, *Chem. Eur. J.* **2019**, *25*, 11402–11411.
[3] T. Chen, M. Li, J. Liu, *Cryst. Growth Des.* **2018**, *18*, 2765–2783.
[4] I. Alkorta, J. Elguero, A. Frontera, *Crystals* **2020**, *10*, 180.
[5] a) B. F. Hoskins, R. Robson, N. V. Y. Scarlett, *Angew. Chem. Int. Ed.* **1995**, *34*, 1203; b) D. B. Leznoff, B.-Y. Xue, B. O. Patrick, V. Scanchez, R. C. Thompson, *Chem. Commun.* **2001**, 259; c) E. Colacio, F. Lloret, R. Kivekäs, J. Ruiz, J. Suárez-Varela, M. R. Sundberg, *Chem.Commun.* **2002**, 592; d) D. B. Leznoff, B.-X. Xue, R. J. Batchelar, F. W. B. Einstein, B. O. Patrick, *Inorg. Chem.* **2001**, *40*, 6026; e) J. Ponce-de-León, R. Infante, M. Pérez-Iglesias, P. Espinet, *Inorg. Chem.* **2020**, *59*, 16599–16610; f) G. Moreno-Alcántar, L. Turcio-García, J. M. Guevara-Vela, E. Romero-Montalvo, T. Rocha-Rinza, A. M. Pendás, M. Flores-Álamo, H. Torrens, *Inorg. Chem.* **2020**, *59*, 8667–8677; g) S. Pawlédzio, M. Malinska, F. Kleemiss, S. Grabowsky, K. Woźniak, *Inorg. Chem.* **2022**, *61*, 4235–4239.
[6] a) H. Schmidbaur, A. Schier, *Chem. Soc. Rev.* **2012**, *41*, 370–412; b) H. Schmidbaur, H. G. Raubenheimer, *Angew. Chem. Int. Ed.* **2020**, *59*, 14748–14771; c) R. P. Herrera, M. C. Gimeno, *Chem. Rev.* **2021**, *121*, 8311–8363; d) Q. Zheng, S. Borsley, G. S. Nichol, F. Duarte, S. L. Cockroft, *Angew. Chem. Int. Ed.* **2019**, *58*, 12617–12623.
[7] a) P. Pyykkö, Y. Zhao, *Angew. Chem. Int. Ed.* **1991**, *30*, 604–605; b) S.-G. Wang, W. H. E. Schwarz, *J. Am. Chem. Soc.* **2004**, *126*, 1266–1276.
[8] a) Q.-M. Wang, D.-Z. Liao, Z.-H. Jiang, S.-P. Yana, P. Cheng, *New J. Chem.* **2004**, *28*, 1347–1351; b) A. Wuttke, M. Feldt, R. A. Mata, *J. Phys. Chem. A* **2018**, *122*, 6918–6925.
[9] a) P. Pyykko, *Chem. Rev.* **1997**, *97*, 597; b) M. A. Rawashdeh-Omary, M. A. Omary, H. H. Patterson, *J. Am. Chem. Soc.* **2000**, *122*, 10371; c) E. Priola, G. Volpi, R. Rabezzana, E. Borfecchia, C. Garino, P. Benzi, A. Martini, L. Operti, E. Diana, *Inorg. Chem.* **2020**, *59*, 203–213; d) E. Priola, G. Mahmoudi, J. Andreo, A. Frontera, *Chem. Commun.* **2021**, *57*, 7268–7271.
[10] a) R. E. Cramer, D. W. Smith, W. Van Doorne, *Inorg. Chem.* **1998**, *37*, 5895. M. A. Rawashdeh-Omary, M. A. Omary, G. E. Shankle, H. H. Patterson, *J. Phys. Chem. B* **2000**, *104*, 6143; b) M. A. Omary, H. H. Patterson, *J. Am. Chem. Soc.* **1998**, *120*, 7696; c) R. L. W. Morris, M. Stender, D. S. Tinti, A. L. Balch, *Inorg. Chem.* **2003**, *42*, 3237.
[11] a) J. M. Forward, Z. Assefa, J. P. Fackler, Jr., *J. Am. Chem. Soc.* **1995**, *117*, 9103; b) M. A. Rawashdeh-Omary, M. A. Omary, H. H. Patterson, J. P. Fackler, Jr., *J. Am. Chem. Soc.* **2001**, *123*, 11237; c) M. Stender, M. M. Olmstead, A. L. Balch, D. Rios, S. Attar, *Dalton Trans.* **2003**, 4282.
[12] a) D. B. Leznoff, B.-Y. Xue, C. L. Stevens, A. Storr, R. C. Thompson, B. O. Patrick, *Polyhedron* **2001**, *20*, 1247; b) E. Colacio, F. Lloret, R. Kivekas, J.

Suárez-Varela, M. R. Sundberg, R. Uggle, *Inorg. Chem.* **2003**, *42*, 560; c) W. Dong, L.-N. Zhu, Y.-Q. Sun, M. Liang, Z.-Q. Liu, D.-Z. Liao, Z.-H. Jiang, S.-P. Yan, P. Cheng, *Chem. Commun.* **2003**, 2544; d) M. J. Katz, D. B. Leznoff, *J. Am. Chem. Soc.* **2009**, *131*, 18435–18444; e) M. J. Katz, H. Kaluarachchi, R. J. Batchelor, A. A. Bokov, Z.-G. Ye, D. B. Leznoff, *Angew. Chem. Int. Ed.* **2007**, *46*, 8804–8807.
[13] a) Y. Guo, Y. Ma, N. Zhou, Z.-Q. Liu, Q.-L. Wang, S.-P. Yan, D–Z. Liao, *ZAAC* **2010**, *636*, 865–871; b) H.-B. Zhou, S.-P. Wang, Z.-Q. Liu, D.-Z. Liao, Z.-H. Jiang, S.-P. Yan, P. Cheng, *Inorg. Chim. Acta* **2006**, *359*, 533–540; c) D. Zhang, H. Wang, L. Tian, J. Jiang, Z.-H. Ni, *CrystEngComm* **2009**, *11*, 2447–2451.
[14] R. F. W. Bader, *Chem. Rev.* **1991**, *91*, 893–928.
[15] E. R. Johnson, S. Keinan, P. Mori-Sánchez, J. Contreras-García, A. J. Cohen, W. Yang, *J. Am. Chem. Soc.* **2010**, *132*, 6498–6506.
[16] E. D. Glendening, C. R. Landis, F. Weinhold, *WIREs Comput. Mol. Sci.* **2012**, *2*, 1–42.
[17] K. Kitaura, K. Morokuma, *Int. J. Quantum Chem.* **1976**, *10*, 325–340.
[18] a) L. J. Farrugia, H. M. Senn, *J. Phys. Chem. A* **2010**, *114*, 13418–13433; b) F. Cortes-Guzman, R. F. W. Bader, *Coord. Chem. Rev.* **2005**, *249*, 633–662.
[19] L. Ould-Moussa, M. Castellà-Ventura, E. Kassab, O. Poizat, D. P. Strommen, J. R. Kincaid, *J. Raman Spectrosc.* **2020**, *31*, 77–390.
[20] a) A. Ozel, S. Kecel Gunduz, S. Akyuz, *J. Mol. Struct.* **2007**, *834*, 548–554; b) K. Burger, F. E. Wagner, A. Vértes, É. Bencze, J. Mink, I. Labàdi, Z. Nemes-Vetéssy, *J. Phys. Chem. Solids* **2001**, *62*, 2059–2068.
[21] K. Nakamoto, *Infrared and Raman Spectra of Inorganic and Coordination Compounds, Part B: Applications in Coordination, Organometallic, and Bioinorganic Chemistry*, John Wiley & Sons, 2009.
[22] a) C. J. Shorrock, B.-Y. Xue, P. B. Kim, R. J. Batchelor, B. O. Patrick, D. B. Leznoff, *Inorg. Chem.* **2002**, *41*, 6743–6753; b) S. F. A. Kettle, E. Diana, E. M. C. Marchese, E. Boccaleri, G. Croce, T. Sheng, P. L. Stanghellini, *Eur. J. Inorg. Chem.* **2010**, 3920–3929; c) G. A. Bowmaker, K. C. Lim, B. W. Skelton, A. H. White, *Z. Naturforsch. B* **2004**, *59*, 1264–1276.
[23] E. Priola, G. Volpi, R. Rabezzana, E. Borfecchia, C. Garino, P. Benzi, A. Martini, L. Operti, E. Diana, *Inorg. Chem.* **2020**, *59*, 203–213.
[24] E. Espinosa, E. Molins, C. Lecomte, *Chem. Phys. Lett.* **1998**, *285*, 170–173.
[25] CrysAlisPRO, Version 1.171.36.20, Oxford Diffraction Agilent Technologies UK Ltd, Yarnton, England.
[26] G. M. Sheldrick, *Acta Crystallogr.* **2015**, *C71*, 3–8.
[27] A. L. Spek, *J. Appl. Crystallogr.* **2003**, *36*, 7–13.
[28] R. Ahlrichs, M. Bär, M. Hacer, H. Horn, C. Kömel, *Chem. Phys. Lett.* **1989**, *162*, 165–169.
[29] C. Adamo, V. Barone, *J. Chem. Phys.* **1999**, *110*, 6158–6170.
[30] S. Grimme, J. Antony, S. Ehrlich, H. Krieg, *J. Chem. Phys.* **2010**, *132*, 154104.
[31] F. Weigend, *Phys. Chem. Chem. Phys.* **2006**, *8*, 1057–1065.
[32] D. Andrae, U. Haeussermann, M. Dolg, H. Stoll, H. Preuss, *Theor. Chim. Acta* **1990**, *77*, 123–141.
[33] T. Lu, F. Chen, *J. Comput. Chem.* **2012**, *33*, 580–592.
[34] J. W. Humphrey, A. Dalke, K. Schulten, *J. Mol. Graphics* **1996**, *14*, 33–38.
[35] T. A. Keith, J. Millam, GaussView, Version 6.0.16, R. Dennington, Semichem Inc., Shawnee Mission, KS, 2019.
[36] E. D. Glendening, J. K. Badenhoop, A. E. Reed, J. E. Carpenter, J. A. Bohmann, C. M. Morales, P. Karafiloglou, C. R. Landis, F. Weinhold, NBO 7.0; Theoretical Chemistry Institute, University of Wisconsin: Madison, WI, USA, 2018.

Manuscript received: January 23, 2023
Revised manuscript received: May 2, 2023
Accepted manuscript online: May 4, 2023